Sizing of an Energy Storage System for Grid Inertial Response and Primary Frequency Reserve

Knap, Vaclav; Chaudhary, Sanjay Kumar; Stroe, Daniel Loan; Swierczynski, Maciej Jozef; Craciun, Bogdan-Ionut; Teodorescu, Remus

Published in:
I E E E Transactions on Power Systems

DOI (link to publication from Publisher):
10.1109/TPWRS.2015.2503565

Publication date:
2016

Document Version
Accepted author manuscript, peer reviewed version

Sizing of an Energy Storage System for Grid Inertial Response and Primary Frequency Reserve

Vaclav Knap, *Member, IEEE,* Sanjay K. Chaudhary, *Member, IEEE,* Daniel-Ioan Stroe, *Member, IEEE,* Maciej Swierczynski, *Member, IEEE,* Bogdan-Ionut Craciun, and Remus Teodorescu *Fellow, IEEE*
Department of Energy Technology, Aalborg University, Aalborg, Denmark

***Abstract*—Large-scale integration of renewable energy sources in power system leads to the replacement of conventional power plants (CPPs) and consequently challenges in power system reliability and security are introduced. This study is focused on improving the grid frequency response after a contingency event in the power system with a high penetration of wind power. An energy storage system (ESS) might be a viable solution for providing inertial response and primary frequency regulation. A methodology has been presented here for the sizing of the ESS in terms of required power and energy. It describes the contribution of the ESS to the grid, in terms of inertial constant and droop. The methodology is applied to a 12-bus grid model with high wind power penetration. The estimated ESS size for inertial response and primary frequency regulation services are validated through real-time simulations. Moreover, it is demonstrated that the ESS can provide the response similar to that provided by the CPPs.**

***Index Terms*—Energy storage, Frequency response, Inertia, Primary frequency regulation, Stability, Wind power generation.**

I. Introduction

THE concern for climate change, sustainability and energy security has driven the development of renewable energy sources (RESs) industry. Large RESs, especially wind and photovoltaic power plants, have been installed in Europe and USA. As the penetration of RES is growing in the power system network, the fossil-fuel based conventional power plants (CPPs) are getting decommissioned [1]. Such a replacement of CPPs by wind and photovoltaic power plants affects the power system behavior. The CPPs are based on synchronous generators, which inherently exhibit inertial response (IR) to sudden frequency deviations. Further, if spinning reserves are available, they participate in the load-frequency regulation as defined by their droop characteristics. Unlike, the CPPs, the RES-based plants are connected to the grid through power electronic converters [2]. Such power electronic interfaces decouple the grid frequency from the speed of the rotating machines in wind power plants (WPPs). Moreover, the photovoltaic power plants (PVPPs) have static dc generators. Therefore, the RES-based plants, by themselves, neither provide the inertial response nor participate in load-frequency regulation and their integration at large scale can lead to loss of IR and primary frequency reserve (PFR).

WPPs and PVPPs are usually operated with maximal power point tracking at maximal power. Some reserve has to be maintained, if these plants are expected to provide IR or PFR. Methods for providing IR and/or PFR from RES-based plants by curtailing their power generation are proposed in [2]–[5]. However, by following this approach the RES maximal power capability is not used, which is highly undesirable. According to [2], [5], the WPPs can provide IR by using their stored kinetic energy. However, there is only a momentary increase in the output power, as it is accompanied by a decrease in the rotor speed, and hence a change of the operating point. The time duration of this support is usually very short in the range of 10 seconds. Moreover, it might result in a second frequency dip, while the rotor speed is recovering. Such an event can be dangerous for the grid stability [6]. In [7], the authors have investigated the use of the HVDC technology for providing IR by varying the DC voltage. The use of demand side management (DSM) technique for grid frequency support is studied in [2]. Specifically for the IR, it can be realized by multi-stage underfrequency load shedding [8] or by domestic thermostatic load [9]. Moreover, the DSM approach is suitable for providing PFR by thermostatically controlled loads [10] or by heat pump water heaters [11], [12]. Nevertheless, DSM would require additional infrastructure like smart devices and communication infrastructure. Upcoming concepts such as vehicle-to-grid and grid-to-vehicle are introducing electric vehicles (EVs) as a source for frequency support [12], [13]; however, the infrastructure does not exist yet and the fleet of EVs is currently too small to support the grid. Furthermore, energy storage systems (ESSs), which offer a variety of storage technologies [14], represent a suitable alternative for providing both IR [15], [16], and PFR [11], [12], [17], [18]. This solution might be economically more viable than the curtailment of RESs or load shedding [19].

Tielens proposed providing IR and PFR from RESs extended by an ESS in [2]. In [16], the ESS was used for the IR and it was sized to deliver arbitrarily chosen rated power for at least 15 seconds. In order to size the ESS for the IR in [15], a set of simulation for various ESS sizes was performed and the final size was picked according to results fulfilling the target limits of a rate of change of frequency and minimum frequency in the system. Yue, in [20], used a probabilistic approach in order to size the ESS for the IR required for frequency variations caused by high solar penetration in the system, which was carried out by performing a high number of simulations. A control strategy for an ESS providing IR and PFR in micro-grids was proposed in [21]; however, sizing the ESS was out of the scope of that investigation. To meet a specific frequency response, a number of simulations with various ESS sizes were performed in [12] and a relation between the ESS size and frequency deviation was derived for the studied system. A methodology for sizing a battery ESS, for providing PFR in a micro-grid, based on battery overloading characteristics and power mismatch was

introduced in [22]. Optimization of the ESS size to provide the PFR was done and presented in [18] for the profit maximizing at the ancillary service market. All the methodologies from the aforementioned studies are based on multiple simulation runs and optimization techniques. Furthermore, they do not indicate their impact upon the overall frequency dynamics. This work proposes an ESS sizing methodology using the system parameters, namely the inertia constant H and the power/frequency characteristic λ. These parameters are used by the system operators to assess the overall system frequency dynamics subsequent to a generator or load contingency [23]. The targeted value of inertia constant, H_{target}, for the inertial response and power/frequency characteristics, λ_{target}, are used in the estimation of power and energy ratings of the ESS. Afterwards, it is demonstrated through simulations that the targeted frequency dynamics are achieved by the ESS system. The theoretically estimated values were verified by real-time simulations considering a realistic power system model.

The structure of the paper is as follows. Section II-A provides a theoretical background regarding the frequency response characteristics of the grid. The frequency response metrics and limits are described in Section II-B. Section II-C presents the proposed methodology for sizing the ESS. The power system under study is presented in section III. Section IV describes the modeling and the control strategy of the ESS. The frequency services provided by an ESS and the ESS sizing processes are presented in Section V. The obtained results are discussed throughout Section VI and the paper is concluded in Section VII. The governor and turbine models are given in the Appendix.

II. Grid Frequency Response and ESS Sizing Methodology

A. Grid Frequency Characteristics

Usually, there are several stages of frequency response behavior subsequent to an event causing a power unbalance in a grid. These stages are illustrated in Fig. 1 for the ENTSO-E system [23]. The first stage is the IR, which is the inherent releasing of energy at the synchronous machines. This stage is followed by the PFR to stabilize the frequency to a steady-state value with an allowed error from its nominal value. The magnitude and time of deployment of these two services influence the frequency nadir, which is the point of minimum frequency in the grid frequency response. This point is relevant to the frequency stability of the grid. Afterward, the secondary frequency reserve (SFR) appears to relieve the PFR, and then, the tertiary frequency reserve (TFR) re-schedules the previous generation.

The scope of this work is to study the IR and PFR when they are provided by an ESS. Moreover, the study is focused on power-outage and underfrequency events and therefore, the rate of change of frequency (ROCOF, $\frac{df}{dt}$) is expressed and presented only as an absolute number, with the meaning of rate of fall of frequency. The effect of loads and damping are neglected. Two main characteristics connected to the frequency response are analyzed in this work: the inertial constant (H) and power/frequency characteristic (λ). The inertia constant of a synchronous machine is defined in [24] as:

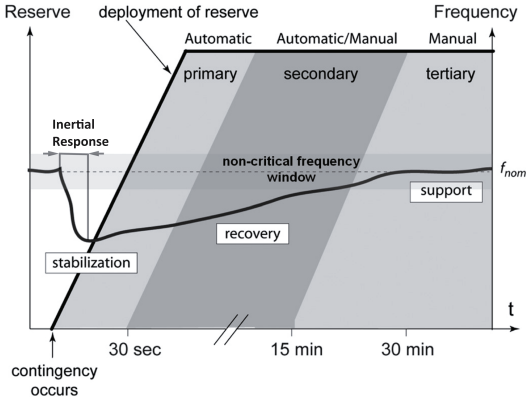

Fig. 1. Stages of frequency response by European Network of Transmission System Operators for Electricity (ENTSO-E) [18].

$$H = \frac{E_{kinetic}}{S_{rated}} = \frac{1}{2}\frac{J \cdot \omega^2}{S_{rated}}, \tag{1}$$

where $E_{kinetic}$ is the stored kinetic energy of a synchronous machine rotor with the rotational speed (ω), moment of inertia (J) and nominal power rating (S_{rated}).

In a power system, containing n number of generating units, the equivalent system inertia constant (H_{sys}) is obtained from:

$$H_{sys} = \frac{\sum_{i=1}^{n} H_i \cdot S_i}{S_{sys}}, \tag{2}$$

where H_i and S_i are the inertia constant and the nominal power of the i-th unit, respectively and S_{sys} is the rating of a specific power system.

The swing equation (3), describes the relation of H_{sys} to the ROCOF ($\frac{df}{dt}$) in a system with the nominal frequency (f_0) due to a power deficit (ΔP_b), which is caused by an unbalance between the active power generation (P_g) and demand (P_l) [24].

$$\frac{2H_{sys}}{f_0}\frac{df}{dt} = \frac{P_g - P_l}{S_{sys}} = \frac{\Delta P_b}{S_{sys}}. \tag{3}$$

The droop constant (R) describes the power versus frequency characteristics of the generator speed governor setting and it is defined in [25] as:

$$R_i = -\frac{\Delta f}{f_0} / \frac{\Delta P_i}{S_i}. \tag{4}$$

Finally at the system level, the power/frequency characteristic (λ) is given by (5), which determines the steady-state frequency error [25].

$$\lambda = -\frac{\Delta P}{\Delta f_{ss}} = \sum_{i=1}^{n} \frac{1}{R_i}\frac{S_i}{f_0}, \tag{5}$$

where Δf_{ss} is the steady-state frequency difference from the nominal frequency (f_0) with the change of the active power demand (ΔP), R_i is the droop or regulation and S_i is the nominal power of the i-th generation unit.

These characteristics provide the fundamental estimation about the frequency response in a grid, immediately and for shorter time period, after an unbalance in the active power.

B. Frequency Response: Rate of change of frequency and steady-state frequency

A generator contingency usually results in an instantaneous power deficit and the frequency dynamics is observed. Theoretically, the initial ROCOF, $\frac{df}{dt}$, and steady-state frequency error, Δf_{ss}, can be estimated by (3) and (5) using the system inertia constant (H) and governor droop settings (R). Since

these values continuously vary over the time, the worst case values resulting from the most severe contingency might be considered for the design purpose. These computations serve as a simple and fast estimation of the system response and later on for the ESS size estimation.

Alternatively, when the measurement data are available from field measurements, $\frac{df}{dt}$ and Δf_{ss} can be numerically computed, and then the effective values of H and R can be estimated. In this work, such measurements are obtained from the real time simulation of the grid model, and hence referred as simulated values.

The metrics for frequency response are based on the operational requirements and grid codes. According to the grid code from ENTSO-E [26], the $\frac{df}{dt}$ is important in connection with the ROCOF protection relays and it should not be greater than 0.5 Hz/s. This value of 0.5 Hz/s is used as the reference point in this work. However, no relays are practically implemented in the grid model. Generally, these relays protect the distribution generation and violating of this limit might cause generation loss. According to [27], a ROCOF relay has a typical delay in the range of 50 ms to 500 ms and a measuring windows from 40 ms to 2 s. In this study, the $\frac{df}{dt}$ for the simulation evaluation is computed as an average value of derivation in a time period between 0 and 0.5 s after the generation loss. The minimum instantaneous frequency after loss of generation (f_{min}) is defined as 49.2 Hz [28]. A lower frequency for a certain time period would lead to an underfrequency load shedding; in this case, the specific requirements vary between countries [26], [29]. The minimum acceptable quasi-steady-state frequency (f_{ss}) is considered as 49.8 Hz [28]. The f_{ss} is computed from the frequency of the system in steady-state, since only the PFR has been considered in the present work.

C. Methodology

Fig. 2 presents the methodology to identify the required ESS size (power and energy ratings) for meeting the targets of the provided services. For the sake of generality of the method, no specific ESS technology has been considered here. It can be, however, modified to include the specific characteristics (time response, life-time considerations, etc) and limitations (power and energy) of the ESS technology of interest.

The method uses the preliminary knowledge of the target system, namely system size (S_{sys}), system inertia (H_{sys}), and power/frequency characteristic (λ_{sys}). The user has to decide the target power unbalance (ΔP) and/or ROCOF ($\frac{df}{dt}$) for which the ESS is going to be sized. These defined target values lead to the target system inertial constant (H_{target}) and target system power/frequency characteristic (λ_{target}), according to which the ESS is sized.

The target services demonstrated in this paper are frequency response services: IR and PFR. They are percepted as "high power oriented," with fast response and applicable for the short time periods (up to 15 minutes). The other frequency response services, e.g. SFR and TFR, are considered to be "high energy oriented" and they are usually required for longer time period. They are beyond the scope of this paper.

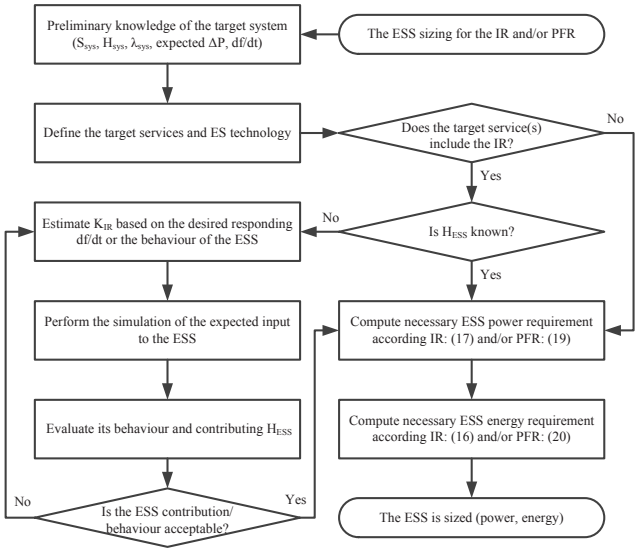

Fig. 2. Flowchart of the used methodology.

TABLE I
THE OVERVIEW OF THE GENERATION UNITS IN THE PS0 AND THEIR SELECTED PARAMETERS.

Power plant	Power rating (S) [MVA]	Active power [MW]	Droop (R) [-]	Inertial constant (H) [s]	Number of units [-]
G1	750	525	0.0500	10.0128	3 / 2**
G2	640	400	0.0500	8.3213	4
G3	384	250	0.0500	6.9344	2
G4	474	300	0.0500	6.6722	3
Total	2248	1475	0.00111*	8.3010*	-
Total**	1998	-	0.00125*	8.0868*	-

*the recomputed equivalent value for the actual PS0

** after the loss of one unit of G1

III. THE POWER SYSTEM UNDER STUDY

The power system under study was based on the generic 12-bus system for wind power integration studies, presented in [30]. It was modeled in RSCAD, and simulated in RTDS system.

The base case power system (PS0) has four CPPs and no WPPs as shown in Fig. 3. Its main parameters are summarized in Table I, where the recomputed equivalent value for the droop R is based on (5) and it was obtained as:

$$\begin{aligned} R_{total} &= \frac{1}{\lambda_{total}} = \frac{f_0}{\sum_{i=1}^{n} \frac{S_i}{R_i}}, \\ R_{PS0} &= \frac{50}{\frac{750}{0.05} + \frac{640}{0.05} + \frac{384}{0.05} + \frac{474}{0.05}} = 0.00111. \end{aligned} \tag{6}$$

The recomputed inertial constant H for the system followed directly (2), and specifically it was obtained as:

$$\begin{aligned} H_{PS0} &= \frac{10.0128 \cdot 750 + 8.3213 \cdot 640 + 6.9344 \cdot 384 + 6.6722 \cdot 474}{2248}, \\ H_{PS0} &= 8.3010 \ s. \end{aligned} \tag{7}$$

The power/frequency characteristic λ_{PS0} of this system is 899.2 MW/Hz before the contingency and 799.2 MW/Hz after the contingency. The parameters for the governor and turbine models of the CPPs are given in the Appendix.

In order to achieve 50 % wind power penetration, the base power system, PS0, was modified by replacing the conventional power plants with wind power plants. The modified system was labeled as PS1. Four group of WPPs with a total

TABLE II
THE OVERVIEW OF THE GENERATION UNITS IN THE PS1 AND THEIR SELECTED PARAMETERS.

Power plant	Power rating (S) [MVA]	Active power [MW]	Droop (R) [-]	Inertial constant (H) [s]	Number of units [-]
G1	750	525	0.0500	10.0128	3 / 2**
G2	320	200	0.0500	8.3213	2
WPP	1178	750	0	0	4
Total	2248	1475	0.00234*	4.5251*	-
Total**	1998	-	0.00305*	3.8384*	-

*the recomputed equivalent value for the actual PS1

** after the loss of one unit of G1

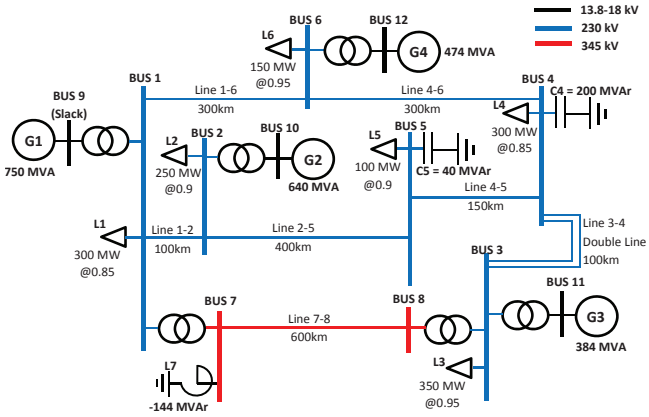

Fig. 3. 12-bus grid model for PS0.

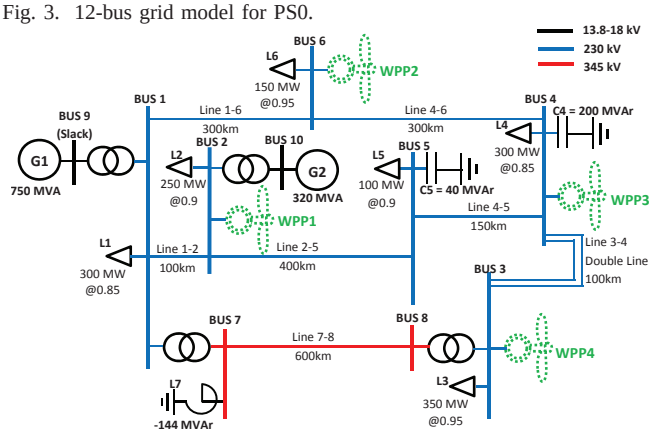

Fig. 4. 12-bus grid model for PS1.

rating of 1178 MVA were connected to the system. The CPPs G3 and G4 were completely removed and G2 was reduced from 4 units to 2 units. The overview of generation units in the PS1 is shown in Table II, the recomputed values were obtained similarly as in (6) and (7). After these changes, the theoretical value of power/frequency characteristic λ_{PS1} of this system, computed according to (5), has reduced to 428 MW/Hz before the contingency and 328 MW/Hz after the contingency. It was assumed that the WPPs do not provide IR and PFR and their active power output remains constant during the study. The overview of the 12-bus grid model in the PS1 scenario is shown in Fig. 4.

A. Generator Contingency

The power system should be planned to withstand contingencies like a loss of a major component [31]. In this work, the outage of the biggest generation unit, G1, in the system has

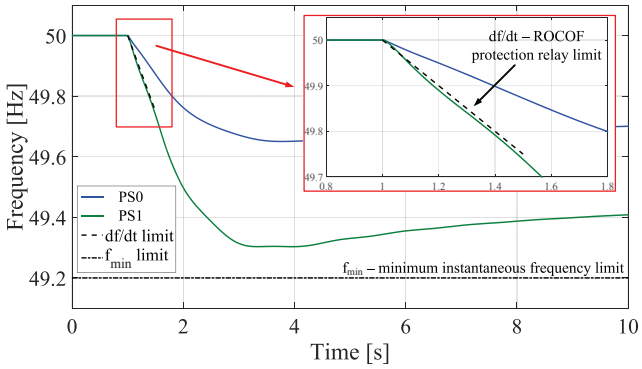

Fig. 5. Frequency responses for the PS0 and PS1

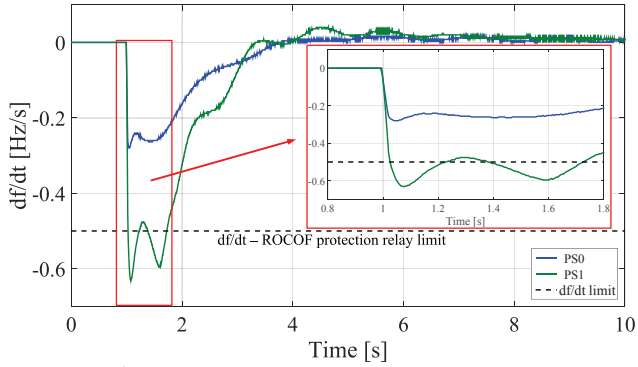

Fig. 6. The $\frac{df}{dt}$ for the PS0 and PS1

TABLE III
THE FREQUENCY RESULTS FOR THE SYSTEMS AFTER SUDDEN GENERATION LOSS.

System	Method	df/dt [Hz/s]	f_{min} [Hz]	f_{ss} [Hz]
PS0	Estimation	0.27	-	49.78
PS0	Simulation	0.25	49.65	49.78
PS1	Estimation	0.57	-	49.47
PS1	Simulation	0.53	49.30	49.46

been considered as the most severe case according to the N-1 contingency for generation outage [23]. It has a nominal rating of 250 MVA. Prior to the event it was producing 175 MW active power in steady-state. The frequency response dynamics was observed in the cases PS0 and PS1, and thus the effect of increased wind power penetration in the frequency dynamics was analysed. Afterwards, an ESS is sized to improve the frequency response.

B. Initial System Studies

The outage of the 250 MVA unit in G1 in the power system models PS0 and PS1 were simulated on the RTDS system. The frequency response and the corresponding ROCOF for these cases are illustrated in Fig. 5 and Fig. 6, respectively. The frequency response metrics the $\frac{df}{dt}$, f_{min} and f_{ss} were computed theoretically and also from simulated data. The obtained results are summarized in Table III, showing a good agreement between the theoretically estimated and the corresponding simulated values. Hence, the system indices for (H) and (R) can be used for quick estimation of the system dynamics. The simulated results are considered more reliable since they account for the multiple machines and the system network. Hence, the inertial constant of PS1 (H_{PS1}) is

recomputed using (3) and using the simulated values of the $\frac{df}{dt}$ (i.e., 0.53 Hz/s). The resultant H_{PS1} is then 4.13 s for the PS1.

The effect on the ROCOF, of introducing high wind power penetration levels in the system, is shown in Fig. 6 and Table III. The $\frac{df}{dt}$ in PS1 is approximately double of the value in the case PS0. The simulated curves show that, in this case, the ROCOF has a more oscillatory nature. The oscillations in the frequency are caused by the generators swinging against each other. The difference between f_{min} and the nominal frequency is exactly two times higher in PS1 than in PS0. Similarly, the f_{ss} difference is 2.4 times higher. When these results are compared with the grid safety limits, one can observe that the limits are violated for the f_{ss} in both systems. However, in the case of PS0, there is a very small difference from the target value. The $\frac{df}{dt}$ in the PS1 is exceeding the allowed limits of 0.5 Hz/s and has to be reduced. The f_{min} is not violated in any of the systems.

IV. Energy Storage System

A. Modeling and control of the ESS

The ESS controller comprises two parts — one for the IR control and the other for the PFR control, as shown in the block diagram in Fig. 7. The two parts can be individually enabled or disabled. The outputs p_{IR} and p_{PFR} are expressed in pu and their negated sum is limited to $\pm$ 1 pu before scaling by the nominal rating S_{ESS} to produce the power P_{ESS} to be injected into the grid. The negated sum is used such that the the power P_{ESS} is positive for falling frequency and negative frequency deviation. Thus, the power injected by the ESS into the grid due to the IR, p_{IR}, and the PFR contribution, p_{PFR}, is given by,

$$\begin{aligned} P_{ESS} &= S_{ESS} \cdot (p_{IR} + p_{PFR}) \\ |P_{ESS}| &\leq S_{ESS} \end{aligned} \tag{8}$$

The actual power exchanged at the ESS, P_{eff}, differs from the power injected into the grid due to charging and discharging efficiency. If the charging efficiency is η_c and the discharging efficiency is η_d, P_{eff} is given by,

$$P_{eff} = \begin{cases} \dfrac{P_{ESS}}{\eta_d}, & \text{for } P_{ESS} > 0 \quad (9a) \\ P_{ESS} \cdot \eta_c, & \text{for } P_{ESS} < 0, \quad (9b) \end{cases}$$

When $P_{eff} > 0$ the ESS gets discharged, and it gets charged when $P_{eff} < 0$. The charging and discharging of the ESS affects its actual state of charge, SOC, which is given by

$$SOC = SOC_{initial} - \frac{\int (P_{eff}) \cdot dt}{E_{ESS}} \cdot 100, \tag{10}$$

where $SOC_{initial}$ is the initial state of charge. For the sake of generalization, the SOC operation region is considered from 0 % to 100 %. After providing the service, the ESS is restored to the $SOC_{initial}$ by the SOC re-establishing strategy as described [32], [33].

B. Primary Frequency Reserve Control

The PFR control follows the UCTE definitions and standards for the continental Europe [28]. The nominal frequency is 50 Hz. The PFR is activated, when frequency deviation exceeds $\pm$20 mHz from the nominal value. The total PFR has to be linearly deployed within 30 s for a frequency deviation of $\pm$200 mHz. The PFR provider has to be capable of delivering the service at least for 15 minutes. The droop R_{ESS} value is equal to 0.0036 in order to deliver the ESS nominal power (S_{ESS}) at $\pm$200 mHz frequency deviation. However, the overall droop for the ESS reaches the constant value of 0.0036 only in the regulated area. When the frequency deviation exceeds $\pm$200 mHz, the ESS gets limited by its maximum power rating, and R_{ESS} varies according (4) as shown in Fig. 8.

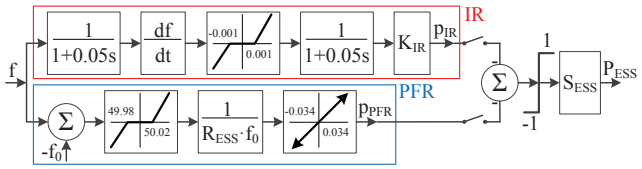

Fig. 7. Block diagram of the ESS control for IR and PFR services.

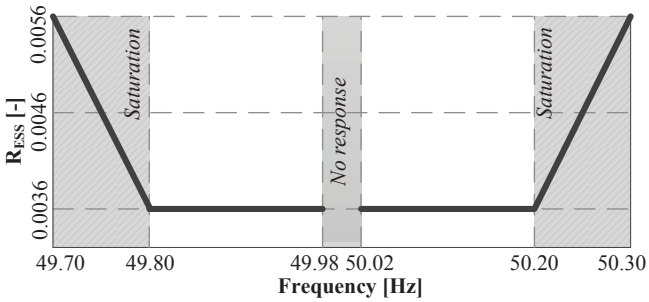

Fig. 8. Effective value of the ESS droop.

C. Inertial Response Control and Effective Inertia Contribution

The IR control of the ESS is based on a derivative control [15], in order to provide synthetic inertia. The deadband prevents the ESS from reacting to small deviations in frequency. First-order low-pass filters filter out the noise from the derivative signal and prevent sudden jumps as well. Moreover, these filters introduce an intentional time delay in the ESS response, which allows the frequency deviation to be observed over a larger part of the grid. Thus, other supportive units can participate in the response as well [5].

The IR contribution of the ESS in the power system frequency dynamics can be assessed, by reformulating the swing equation (3), and defining the ESS inertial constant (H_{ESS}) as follows:

$$H_{ESS} = p_{IR} \cdot \frac{f_0}{2} \cdot \left(\frac{df}{dt}\right)^{-1}. \tag{11}$$

If the influence of the deadband in Fig. 7 is neglected, then the inertial response is proportional to the rate of change of frequency $\frac{df}{dt}$ as follows,

$$p_{IR} = \frac{K_{IR}}{(1 + s\tau_1) \cdot (1 + s\tau_2)} \cdot \left(\frac{df}{dt}\right). \tag{12}$$

where τ_1 and τ_2 are filtering time constants of 0.05 s each. If these time constants are ignored, (11) can be further approximated as,

$$p_{IR} \approx K_{IR} \cdot \left(\frac{df}{dt}\right). \tag{13}$$

Thus, the inertial response can be approximated by a gain, K_{IR} as long as $p_{IR} \leq 1$ pu. Therefore, K_{IR} can be initially estimated according the desired ESS response. For example, if the ESS has to provide the nominal power for $\frac{df}{dt} = 0.5$ Hz/s, then the K_{IR} has to be equal to 2.

The value of H_{ESS} is dependent on the IR control gain K_{IR}. For high values of K_{IR}, the ESS output power might get limited to its rated capacity $|p_{IR}| \leq 1$ pu, the corresponding inertial constant would be lower. Thus, from (11) and (13) the inertial constant H_{ESS} can be approximated as,

$$H_{ESS} \approx \begin{cases} \frac{f_0}{2} \cdot K_{IR}, & \text{for } |p_{IR}| \leq 1 \quad (14a) \\ \frac{f_0}{2} \cdot \left(\frac{df}{dt}\right)^{-1}, & \text{for } |p_{IR}| > 1 \quad (14b) \end{cases}$$

Thus, according to (14) the H_{ESS} remains constant, as long as $|p_{IR}| \leq 1$ and it starts to decrease for high values of $\left|\frac{df}{dt}\right|$ when $|p_{IR}| \leq 1$.

The ESS inertial constant H_{ESS} is expressed as a function of ΔP, which directly affects the $\frac{df}{dt}$ of the system. Fig. 9 provides an overview of the variation of H_{ESS} vs. ΔP for different values of K_{IR}. For $K_{IR} = 1$ and 2, the simulated values of H_{ESS} were found to be 19.81 s and 39.41 s respectively in contrast to the values 25 s and 50 s obtained through (14a); the fact that the inertia values were computed after the contingency event when the delaying effect $\tau_1 = \tau_2 = 0.05$ s cannot be ignored as approximated in (13). For $K_{IR} = 20$, the H_{ESS} is found to be 44.32 s for $\Delta P = 175$ MW.

Based on the analysis of the obtained curves, three possible approaches have been analysed. The first approach is for a gain $K_{IR} = 1$, where the H_{ESS} is constant for the whole range of the simulated power change. The second approach considers a gain $K_{IR} = 2$, where the H_{ESS} remains constant only until the change in the power is equal to the largest generation loss in the studied system (175 MW) and after this point it has a decreasing tendency. In the third approach, K_{IR} is set at 20. In this case, the IR gets limited to $p_{IR} = 1$ pu as soon as $\frac{df}{dt} > 0.05$ Hz/s. The H_{ESS} was compute according to (14b). For different values of power outage, ΔP, the value of H_{ESS} varies as shown in Fig. 9. For $K_{IR} = 20$, H_{ESS} has been approximated by a function, which was fitted for a curve with a coefficient of determination R^2 value equal to 0.9991.

$$H_{KIR.20}(\Delta P) = 1.736 \cdot 10^4 \cdot \Delta P^{1.156}. \quad (15)$$

Such a function can be used in the frequency response analysis of the system during contingencies.

The ESS power output for these three values of K_{IR} , due to the contingency of G1 which caused a power deficit of 175 MW, is shown in Fig. 10. The IR lasts for a few seconds as shown in Fig. 1. The energy delivered by the ESS during the IR can be obtained by integrating the area under the power curve for the duration between the contingency event and the first zero-crossing. The zero crossing indicates that $\frac{df}{dt}$ has changed its sign and hence the need for IR is over in most of the cases involving single contingency events. In the event of load outage, the frequency will increase, and the ESS will have to contribute to IR by absorbing power, i.e. $p_{IR} < 0$, which implies charging of the ESS.

The ESS should have stored energy ESS_{up} so that it can discharge and provide $p_{IR} > 0$ during generator outages and subsequent frequency fall, while it should be able to absorb energy, ESS_{dn}, by drawing power from the grid and get charged. Therefore, accounting for the ESS efficiency and

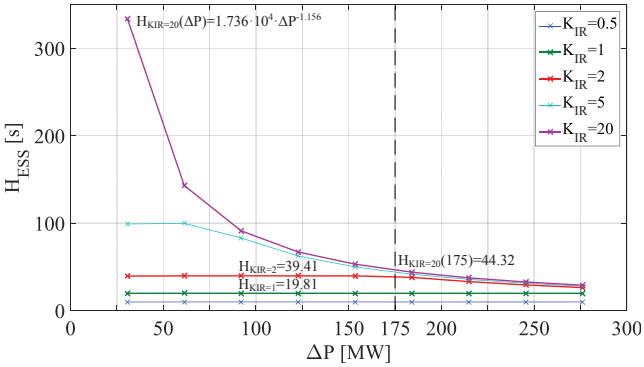

Fig. 9. Inertial constant of the ESS, H_{ESS}, for the different K_{IR} dependent on change in the power.

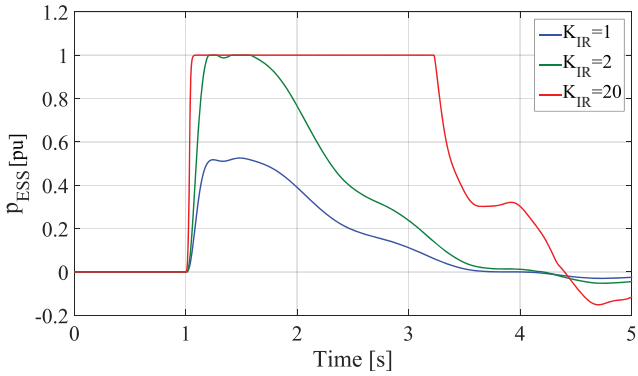

Fig. 10. The ESS power output (p_{ESS}) for selected K_{IR} and for power change of 175 MW.

10 % tolerance margin, the ESS nominal energy capacity is given by,

$$E_{ESS} = ESS_{up} + ESS_{dn} = (\int_b^e p_{ESS}(t)dt \cdot \eta_c + \\ + \int_b^e p_{ESS}(t)dt/\eta_d) \cdot 1.1 \cdot S_{ESS}, \quad (16)$$

where, b is the beginning time of providing the IR. e is the ending time of providing the IR, indicated by the first zero-crossing of the ESS power output (p_{ESS}).

The ESS is controlled here using a derivative controller to provide the IR in such a way, that it emulates the inertial response of synchronous machine and its inertial constant was determined. Alternative approaches for providing the IR, which are different from that of a synchronous machine, were proposed in [5], [34].

V. Frequency Response Services Provided by an ESS

According to the ENTSOE grid code, the maximum values of the ROCOF $\left|\frac{df}{dt}\right| \leq 0.5$ Hz/s and of the steady state frequency error $|\Delta f_{ss}| \leq 0.2Hz$ for the 50 Hz system under study were selected as the design objective. The outage of generator G1 and subsequent power deficit of $\Delta P = 175MW$ is considered the biggest contingency event.

A generalized model of energy storage technology is considered. Losses are incurred during both the charging and discharging of the ESS. Assuming equal charging and discharging efficiency, i.e. $\eta_c = \eta_d = \eta$, gives the round-trip efficiency as $\eta_c \cdot \eta_d = \eta^2$ [14], which was assumed to be 85%.

The actual contingency size depends upon the system configuration. In this work, a contingency of 175 MW has been considered as the biggest contingency event for both

the load and generator outage. Therefore, the ESS is considered to provide identical services in the event of generator contingency, which needs frequency support upwards and in the event of load outage contingency, which needs frequency support downwards. Therefore, for a round-trip efficiency of $\eta^2 = 85\%$, the initial SOC level of the ESS has to be set at $SOC_{initial} = 54\%$.

The power system PS1 with an ESS for different scenarios of IR and PFR services provided from the ESS are listed in Table IV as PS1A - PS1E, together with the parameters of the ESS and simulation results. The ESS output power profiles are shown in Fig. 11 and the frequency profiles are presented in Fig. 12.

A. The IR with ESS

The ESS in this subsection is considered to be used only for providing IR. According to (2), $\left|\frac{df}{dt}\right| \leq 0.5$ Hz/s for $\Delta P = 175$ MW implies a target inertial constant (H_{target}) of 4.4688 s. The power rating of the PS1 after the generation loss (S_{PS1}), as shown in Table II, is 1998 MVA and H_{PS1}= 4.13 s, as computed in Section III-B. Selecting $K_{IR} = 1$, which relates to $H_{ESS} = 19.81$ s (Fig. 9), the required size of the ESS can be estimated using (2) as follows,

$$\begin{aligned} S_{ESS} &= S_{PS1} \cdot \tfrac{H_{target} - H_{PS1}}{H_{ESS} - H_{target}}, \\ &= 1998 \cdot \tfrac{4.4688 - 4.13}{19.81 - 4.4688}, \\ &= 44.13\ MW. \end{aligned} \tag{17}$$

The total energy supplied during the IR against the generator outage was found to be $1.9222 \cdot 10^{-4}$ pu. Assuming that the ESS should be capable of absorbing the same energy amount from the grid, and adding a margin of 10%, the nominal energy rating of the ESS turns out to be 0.0187 MWh.

The power and energy ratings for the ESS for the three representative values of K_{IR} have been computed using (16) and (17) and the results are summarized in Table IV.

For all PS1A, PS1B and PS1C, the $\frac{df}{dt}$ fulfils the operation limits and the resulting ROCOF is even lower than expected. In comparison to PS1A and PS1B, the case PS1C shows an improvement in f_{min}. Even though the ESS got saturated to 1 pu, the power was provided over a longer duration (Fig. 11) due to the high value of K_{IR} and it resulted in a higher demand of energy. Nevertheless, the PS1C has the lowest requirement for the ESS size, i.e. 16.99 MW. The major limitation of the PS1C is the non-linear behavior of its inertial constant, H_{ESS}, which varies with the size of power mismatch (ΔP) in a contingency. In PS1B with $K_{IR} = 2$, the requirement for the ESS power rating is 14%, i.e. 2.38 MW, higher than in PS1C, but the H_{ESS} parameter remains constant during the operation. The energy requirement is lower by 39%. In PS1A, the ESS is not optimally utilized, as with $K_{IR} = 1$ and the H_{ESS} is only 19.81 s, so the ESS power rating requirement of 44.13 MW is more than two times higher than in the PS1C scenario. Even the energy rating is higher than that in PS1B. Therefore, the case PS1B with $K_{IR} = 2$ was chosen to be used for providing IR+PFR services in the case PS1E.

TABLE IV
THE FREQUENCY RESULTS FOR THE SYSTEMS AFTER SUDDEN GENERATION LOSS WITH THE ESS COMPENSATION.

Case	Service	S_{ESS} [MW]	E_{ESS} [MWh]	df/dt [Hz/s]	f_{min} [Hz]	f_{ss} [Hz]
PS1A	**IR**$_{K_{IR}=1}$	44.13	0.0187	0.46	49.32	49.46
PS1B	**IR**$_{K_{IR}=2}$	19.37	0.0163	0.47	49.32	49.46
PS1C	**IR**$_{K_{IR}=20}$	16.99	0.0269	0.47	49.35	49.46
PS1D	**PFR**	98.5	49.5	0.52	49.33	49.78
PS1E	**IR**$_{K_{IR}=2}$ **+PFR**	98.5	49.6	0.34	49.40	49.78

B. The PFR with ESS

In the case PS1D, the PFR is considered as the only service provided by the ESS. The target value for the f_{ss}, after the loss of 175 MW of active power generation, is 49.8 Hz. Following (5), the target power/frequency characteristic (λ_{target}) is obtained as:

$$\lambda_{target} = -\frac{175}{-0.2} = 875 MW/Hz. \tag{18}$$

The value $\lambda_{PS1} = 328$ MW/Hz in the system PS1 is lower than λ_{target}. Therefore, λ_{PS1} has to be increased by the application of PFR service from the ESS. As the targeted frequency is in the regulation area of the ESS, R_{ESS} is considered constant and equal to 0.0036. The necessary power size of the ESS for providing PFR was computed based on (5) as follows:

$$\begin{aligned} S_{ESS} &= (R_{ESS} \cdot f_0) \cdot (\lambda_{target} - \lambda_{PS1}), \\ S_{ESS} &= (0.0036 \cdot 50) \cdot (875 - 328), \\ S_{ESS} &= 98.5\ MW. \end{aligned} \tag{19}$$

The next step is to determine the required energy capacity of the ESS which is necessary for providing PFR. The ESS is assumed to be capable of equally providing upward and downward frequency regulation for 15 minutes. Taking into account the energy storage round-trip efficiency equal to 85 %, the total energy of the ESS is computed as:

$$\begin{aligned} E_{ESS} &= \tfrac{t_{req} \cdot S_{ESS} \cdot \sqrt{\eta_c}}{3600} + \tfrac{t_{req} \cdot S_{ESS}}{3600 \cdot \sqrt{\eta_d}}, \\ E_{ESS} &= \tfrac{900 \cdot 98.5 \cdot \sqrt{0.85}}{3600} + \tfrac{900 \cdot 98.5}{3600 \cdot \sqrt{0.85}}, \\ E_{ESS} &= 49.5\ MWh. \end{aligned} \tag{20}$$

The PFR from the ESS was based strictly on grid code requirements [28]. Different ESS technologies might be capable to provide the PFR faster and more flexible as they may have lower time constants and faster reaction time [14]. This can further improve the grid stability.

C. The IR and PFR with ESS

Usually the IR and PFR stages are separated in time domain as shown in Fig. 1. However, these two services may partially or fully overlap. Consequently, sizing calculations have to be done for both services, the IR and the PFR, but only the higher power requirement is considered for the ESS size determination. In the case PS1E, the requirement is imposed by the PFR service, which is equal to 98.5 MW. Based on the results from the IR sizing, only the K_{IR} = 2 is taken into account for calculations. The IR requirement for energy has to be recomputed for the actual ESS nominal power. The

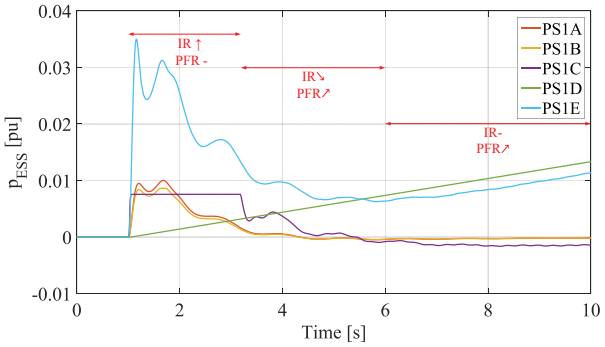

Fig. 11. ESS power output per units of the power system rating after the generation loss, 2248 MVA.

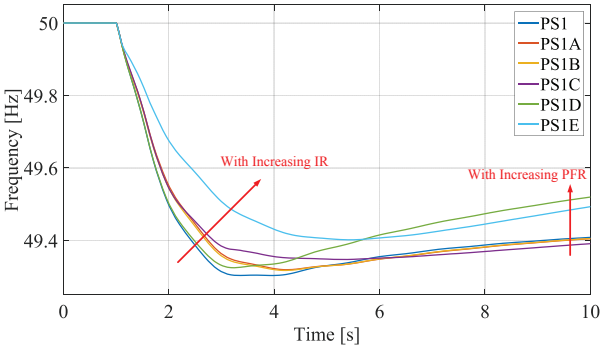

Fig. 12. Frequency profiles for the studied power systems with high wind power penetration and application of the ESS.

total ESS energy requirement of 49.6 MWh, is obtained by summing the requirements for the IR and the PFR. The ESS power output for the PS1E scenario, shown in Fig. 11, has a similar characteristic as the power output of a CPP, which traditionally provides both IR and PFR.

During the frequency recovery period after the nadir has reached, the power from IR is opposite to that of the PFR. Such circumstances can be avoided by blocking the IR, when IR and PFR have opposite signs.

VI. Discussion

The IR service from the ESS in the cases PS1A - PS1C improved the $\frac{df}{dt}$ metric and in the case of PS1C also the f_{min}. In PS1D, not only the f_{ss} was improved, as it was the target of the PFR service, but also the $\frac{df}{dt}$ and f_{min} were improved in comparison to PS1. This is due to the fact that the PFR is linearly activated, when the frequency deadzone is crossed. Hence, it contributes in the first seconds after the event. In PS1E, the ESS provides the same PFR as in PS1D, but additionally it provides the IR from a 98.5 MW ESS. Because of its size, the $\frac{df}{dt}$ and f_{min} are highly improved to 0.34 Hz/s and 49.40 Hz, respectively. The PS1E scenario provides the best results in terms of metrics and it requires the ESS to have a nominal power of 98.5 MW and a nominal energy of 49.6 MWh.

Fig. 12 shows the frequency profiles for the cases PS1A-PS1E. There is a visible improvement in the slowing drop of frequency by increasing IR in the first part. Moreover, the rising steady-state level of frequency in the second part is caused by increasing PFR.

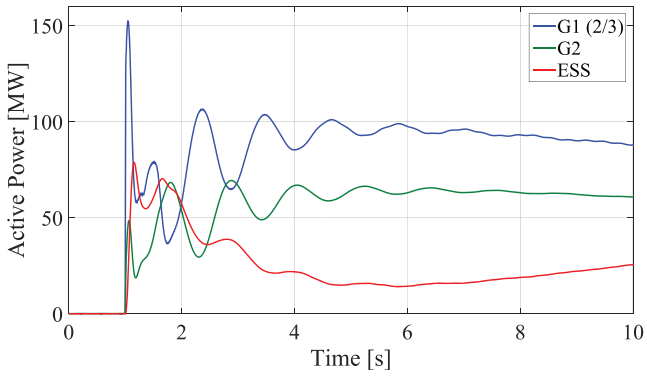

Fig. 13. Comparison of power outputs for the ESS and the CPPs.

The comparison of the CPPs power output and the ESS power output is shown in Fig. 13 for PS1E. The ESS has a slower IR than the G1 and G2 as it was intended according [5] for frequency deviation being seen by both CPPs. Therefore the IR from CPPs is not reduced due to a very fast ESS response. With the actual settings, the PFR from the ESS is also slower than in the case of the CPPs. In the overall picture, the ESS can generate power output similar to the CPPs.

When a contingency leads to a large unbalance in power, the initial rate of change of frequency is determined by the inertia of the rotating machines. The ESS can act only after it has detected the ROCOF. So, when a large number of synchronous generators have been replaced by the RES, the physical inertia of the system will be low, and hence the initial ROCOF will tend to be high. The ESS is expected to provide a fast response to counteract the high ROCOF. In the present implementation (Fig. 7), the rise time (i.e. the time for the output to increase from 10% to 90% of the final value for a step input) for the inertial response controller output is 177.4 ms. Therefore, the high initial $\frac{df}{dt}$ would last for a short period of time before the IR reacts. The ROCOF relays might have to be provided with a dead-time to account for the high initial $\frac{df}{dt}$ in the changed scenario.

VII. Conclusion

The paper identifies possible effects of high RES integration on the power system frequency response. The IR and the PFR in power systems with high RES penetration are lowered and when a contingency appears, the frequency operational limits are exceeded. For supporting the frequency response, ESSs represent a suitable solution for providing IR and PFR.

This paper presents a method for estimating the ESS size in terms of power and energy so as to achieve the targeted system inertia and power/frequency characteristics by providing IR and PFR. In comparison to the IR service, the PFR service requires much larger power and energy ratings of the ESS as it has to provide regulating power for 15 minutes, while the IR is active only for a few seconds. It is demonstrated that the same ESS can be used to provide both the IR and PFR. A generalized model of ESS was used in this study. Specific details pertaining to particular energy storage technology can be included afterwards in particular studies.

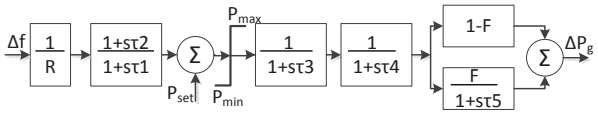

Fig. 14. Block diagram for governor and turbine model.

TABLE V
THE PARAMETERS OF GOVERNORS AND TURBINE'S MODELS.

Power plant	$\tau 1$	$\tau 2$	$\tau 3$	$\tau 4$	$\tau 5$	F
G1	0.15	0	0.1	0.3	10	0.237
G2	0.083	0	0.2	0.05	5	0.28
G3	0.2	0	0.3	0.09	10	0.25
G4	124.47	8.59	0.25	0	0.74	-2

	Fossil steam unit	Hydro unit
$\tau 1$	Governor response time	Control time constant
$\tau 2$	Pilot valve time	Hydro reset time constant
$\tau 3$	Servo time constant	Servo time constant
$\tau 4$	Steam valve bowl time constant	0 for hydro governor
$\tau 5$	Steam reheat time constant	Water starting time constant for hydro governor
F	Shaft output ahead of reheater	Max gate velocity for hydro turbine

In order to fulfill all operational requirements in the studied power system rated at 2248 MVA with high RES penetration of 1178 MVA, (which is slightly over 50 %), it has been found that an ESS of 98.5 MW and 49.6 MWh is needed for providing both IR and PFR. Moreover, it was shown that the ESS can provide a similar response as a CPP does.

APPENDIX
GOVERNORS AND TURBINES DATA

The governors and turbines models of the CPPs are shown in Fig. 14 [35], where Δf stands for measured frequency deviation, R for droop, $\Delta P_{\rm set}$ for the change in load set point and $\Delta P_{\rm g}$ for the change of output power. Their parameters settings are listed in Table V.

REFERENCES

[1] "Scenario Outlook And Adequacy Forecast 2014-2030," European Network of Transmission System Operators for Electricity (ENTSO-E), Tech. Rep., June 2014.

[2] P. Tielens and D. V. Hertem, "Grid Inertia and Frequency Control in Power Systems with High Penetration of Renewables," in *Young Researchers Symp. in Elect. Power Eng.*, vol. 6, Delft, The Netherlands, Apr. 2012.

[3] H. Xin *et al.*, "A New Frequency Regulation Strategy for Photovoltaic Systems Without Energy Storage," *IEEE Trans. Sustain. Energy*, vol. 4, no. 4, pp. 985–993, Oct. 2013.

[4] X. Yuan and Y. Li, "Control of variable pitch and variable speed direct-drive wind turbines in weak grid systems with active power balance," *Renewable Power Generation, IET*, vol. 8, no. 2, pp. 119–131, Mar. 2014.

[5] P. W. Christensen and G. C. Tarnowski, "Inertia for Wind Power Plants - state of the art review - year 2011," in *10th Int. Workshop on Large-Scale Integration of Wind Power into Power Systems*, Aarhus, Denmark, Oct. 2011.

[6] J. Van de Vyver *et al.*, "Droop Control as an Alternative Inertial Response Strategy for the Synthetic Inertia on Wind Turbines," *IEEE Trans. Power Syst*, vol. PP, no. 99, pp. 1–10, 2015.

[7] J. Zhu *et al.*, "Inertia Emulation Control Strategy for VSC-HVDC Transmission Systems," *IEEE Trans. Power Syst.*, vol. 28, no. 2, pp. 1277–1287, May 2013.

[8] W. Gu *et al.*, "Multi-stage underfrequency load shedding for islanded microgrid with equivalent inertia constant analysis," *Int. J. of Elect. Power & Energy Syst.*, vol. 46, pp. 36 – 39, 2013.

[9] V. Trovato *et al.*, "Demand response contribution to effective inertia for system security in the GB 2020 gone green scenario," in *Innovative Smart Grid Technologies Europe (ISGT EUROPE), 2013 4th IEEE/PES*, Oct. 2013, pp. 1–5.

[10] P. Douglass *et al.*, "Smart Demand for Frequency Regulation: Experimental Results," *IEEE Trans. Smart Grid*, vol. 4, no. 3, pp. 1713–1720, Sept. 2013.

[11] T. Masuta *et al.*, "System frequency control by Heat Pump Water Heaters (HPWHs) on customer side based on statistical HPWH model in power system with a large penetration of renewable energy sources," in *Power Syst. Technology (POWERCON), 2010 Int. Conf. on*, Oct. 2010, pp. 1–7.

[12] T. Masuta and A. Yokoyama, "Supplementary Load Frequency Control by Use of a Number of Both Electric Vehicles and Heat Pump Water Heaters," *IEEE Trans. Smart Grid*, vol. 3, no. 3, pp. 1253–1262, Sept. 2012.

[13] Y. Mu *et al.*, "Primary Frequency Response From Electric Vehicles in the Great Britain Power System," *IEEE Trans. Smart Grid*, vol. 4, no. 2, pp. 1142–1150, June 2013.

[14] D.-I. Stroe *et al.*, "Short term energy storage for grid support in wind power applications," in *Optimization of Elect. and Electron. Equipment (OPTIM), 2012 13th Int. Conf. on*, May 2012, pp. 1012–1021.

[15] V. Knap *et al.*, "Grid Inertial Response with Lithium-ion Battery Energy Storage Systems," in *Ind. Electron. (ISIE), 2014 IEEE Int. Symp. on*, June 2014, pp. 1813–1818.

[16] G. Delille *et al.*, "Dynamic Frequency Control Support by Energy Storage to Reduce the Impact of Wind and Solar Generation on Isolated Power System's Inertia," *IEEE Trans. Sustain. Energy*, vol. 3, no. 4, pp. 931–939, Oct. 2012.

[17] M. Swierczynski *et al.*, "Field tests experience from 1.6MW/400kWh Li-ion battery energy storage system providing primary frequency regulation service," in *Innovative Smart Grid Technologies Europe (ISGT EUROPE), 2013 4th IEEE/PES*, Oct. 2013, pp. 1–5.

[18] A. Oudalov *et al.*, "Optimizing a Battery Energy Storage System for Primary Frequency Control," *IEEE Trans. Power Syst*, vol. 22, no. 3, pp. 1259–1266, Aug. 2007.

[19] L. Vargas *et al.*, "Wind power curtailment and energy storage in transmission congestion management considering power plants ramp rates," *IEEE Trans. Power Syst*, vol. PP, no. 99, pp. 1–9, 2014.

[20] M. Yue and X. Wang, "Grid inertial response-based probabilistic determination of energy storage system capacity under high solar penetration," *IEEE Trans. Sustain. Energy*, vol. 6, no. 3, pp. 1039–1049, July 2015.

[21] I. Serban and C. Marinescu, "Control strategy of three-phase battery energy storage systems for frequency support in microgrids and with uninterrupted supply of local loads," *Power Electronics, IEEE Transactions on*, vol. 29, no. 9, pp. 5010–5020, Sept 2014.

[22] M. R. Aghamohammadi and H. Abdolahinia, "A new approach for optimal sizing of battery energy storage system for primary frequency control of islanded microgrid," *Int. J. of Elect. Power & Energy Syst.*, vol. 54, no. 0, pp. 325 – 333, 2014.

[23] "Supporting Document for the Network Code on Load-Frequency Control and Reserves," European Network of Transmission System Operators for Electricity (ENTSO-E), Tech. Rep., June 2013.

[24] P. Kundur *et al.*, *Power System Stability and Control*. McGraw-Hill Education, 1994.

[25] P. Schavemaker and L. van der Sluis, *Electrical Power System Essentials*. Wiley, 2008.

[26] "Supporting Document for the Network Code on Operational Security," European Network of Transmission System Operators for Electricity (ENTSO-E), Tech. Rep., Sept. 2013.

[27] C. Ten and P. Crossley, "Evaluation of Rocof Relay Performances on Networks with Distributed Generation," in *Develop. in Power System Protection, 2008. DPSP 2008. IET 9th Int. Conf. on*, Mar. 2008, pp. 523–528.

[28] "Continental Europe Operation Handbook: P1 - Policy 1: Load-Frequency Control and Performance [C]," Union for the Co-ordination of Transmission of Electricity (UCTE), Tech. Rep., 2009, v.3.0, rev15.

[29] *Automatic Underfrequency Load Shedding* , North American Electric Reliability Corporation (NERC) Std. PRC-006-2, 2014.

[30] A. Adamczyk *et al.*, "Generic 12-Bus Test System for Wind Power Integration Studies," in *Proc. of the EPE Joint Wind Energy and T&D Chapters Seminar*. EPE Association, 2012.

[31] P. Kundur *et al.*, "Definition and classification of power system stability IEEE/CIGRE joint task force on stability terms and definitions," *IEEE Trans. Power Syst*, vol. 19, no. 3, pp. 1387–1401, 2004.

[32] M. Swierczynski *et al.*, "Field Experience from Li-Ion BESS Delivering Primary Frequency Regulation in the Danish Energy Market," *ECS Transactions*, vol. 61, no. 37, pp. 1–14, Sep. 2014.

[33] E. Thorbergsson *et al.*, "Primary Frequency Regulation with Li-Ion Battery Based Energy Storage System - Evaluation and Comparison of Different Control Strategies," in *35th Int.l Telecommun. Energy Conf. 'Smart Power and Efficiency' (INTELEC)*, 2013, pp. 178–183.

[34] G. C. Tarnowski, "Coordinated Frequency Control of Wind Turbines in Power Systems with High Wind Power Penetration," Ph.D. dissertation, Technical University of Denmark, Nov. 2011.

[35] J. Machowski *et al.*, *Power System Dynamics: Stability and Control*. Wiley, 2008.